IEEE Access
Multidisciplinary ⋮ Rapid Review ⋮ Open Access Journal

Received January 28, 2022, accepted February 15, 2022, date of publication February 24, 2022, date of current version March 7, 2022.

Digital Object Identifier 10.1109/ACCESS.2022.3154649

Constraint on Bounded Relative Distance for Robust MME Detection in Spaceborne Cluster Flight Netted Radar

MINGFEI XIA[1,2], SHENGBO HU[1,3], TINGTING YAN[1], YANFENG SHI[1], AND JIANAN CAI[1]

[1]Institute of Intelligent Information Processing, Guizhou Normal University, Guiyang 550001, China
[2]School of Mathematical Science, Guizhou Normal University, Guiyang 550001, China
[3]National Space Science Center, Chinese Academy of Sciences (CAS), Beijing 100190, China

Corresponding author: Shengbo Hu (hsb@nssc.ac.cn)

This work was supported in part by the Guizhou Province Education Department Projects of China under Grant KY [2017]031 and Grant KY[2020]007, and in part by the National Natural Science Foundation of China under Grant 61561009.

ABSTRACT In this paper, we investigate the robust maximum-minimum eigenvalue (MME) detection problem caused by this uncertainty of geometric configuration. Firstly, according to the proposed novel concept of spaceborne cluster flight netted radar (SCFNR) integrated cluster flight spacecraft with netted radar recently, we define the robust detector for the uncertainty of geometric configuration due to the mobility in SCFNR and give the condition about robust MME detector. Using the channel gain matrix in one CPI, the closed-form of the lower bound on the test statistic under the presence of target return, and the upper bound under the absence of target return are given respectively. Secondly, using the mobility model about transmitter-receiver pairs in SCFNR, we give the constraint on the bounded relative distance for robust MME detector in SCFNR. Finally, the effectiveness of the proposed constraint is validated through numerical calculations. The results show also that controlling the orbit elements about the transmitter and receiver platforms in SCFNR can make sure the robustness of MME and the relative distance bounded.

INDEX TERMS Maximum minimum eigenvalue (MME), spaceborne cluster flight netted radar (SCFNR), robust MME detector.

I. INTRODUCTION

As a distributed space multi system, the spaceborne cluster flight netted radar (SCFNR) is composed of several spatially separated, mutually independent and cooperative transmitters and receivers of radars in space, which can maintain bounded relative distances between tens or hundreds of kilometers and to keep loose geometry for the entire mission lifetime, so that orbit controlling and relative position sensing for the spacecraft can be performed well [1]–[3]. The netted radar has many inherent advantages. For example, the spatial distribution of the transmitters and receivers can be assigned to specific application of interest. Also, the netted radar can increase sensitivity to improve the detection, tracking and cognition performance [4], [5]. On the other hand, compared with the traditional radar, spaceborne netted radar has advantages of high flexibility, reliability, and anti-stealth ability [6]–[8]. In addition, it also has the advantage of being all-weather, wide coverage, and satisfying specific coverage requirements due to its location in outer space [9], [10]. Hence, we have proposed the novel concept of SCFNR integrated cluster flight spacecraft with the spaceborne netted radar [11], [12].

Target detection is a fundamental component of radar system and is a critical issue in low SNR environment. Similar to spectrum sensing methods of cognitive radio (CR), a lot of algorithms including the energy detection, the matched filtering (MF) and Neyman-Pearson test have been applied to target detection of radar system [13], [14]. Also, many researchers have investigated robust sensing schemes that achieve higher probability of detection and lower probability of false alarm in the presence of noise uncertainty. In this sense, the eigenvalue-based detection techniques outperform most of the other sensing schemes [15], [16]. Recently, the largest eigenvalue-based detector, also known as generalized likelihood ratio test (GLRT) detector also, has been used to detect radar target [17]–[19]. However, these algorithms are susceptible to the noise power uncertainty, because they rely

The associate editor coordinating the review of this manuscript and approving it for publication was Cheng Hu.

on the knowledge of accurate noise power. In practice, there is little priori information about the return signal or the noise power in the target system. In a low-SNR environment, the return signal becomes even more difficult to detect. By contrast, the uncertainty of the noise power does not adversely affect the maximum minimum eigenvalue (MME) detector's performance in CR network [20]–[22]. So, inspired by MME in CR network, we applied MME detection to target detection in SCFNR systems.

However, for SCFNR, the high-speed flight of platform increases the uncertainty of geometric configuration of radar systems. In [12], we have given the mobility model for bistatic radar pair in SCFNR with twin-satellite mode. This means that the target robust detection will face new challenges due to the uncertainty of geometric configuration in SCFNR caused by the mobility of transmitters and receivers. Therefore, this paper is addressed to analyze the robust MME detection caused by the uncertainty of geometric configuration in SCFNR.

To the best of our knowledge, this is the first paper to investigate the robust MME detection problem caused by the uncertainty of geometric configuration in SCFNR. The main contributions of our work are summarized as follows:

(1) Based on the proposed novel concept of SCFNR integrated cluster flight spacecraft with netted radar, a system model for analyzing the robust MME detector is further presented. Establishing a channel gain matrix, a robust detector for the uncertainty of geometric configuration is defined. Using the lower bound of the test statistic under the presence of target return and the upper bound under the absence of target return respectively, the condition for a robust MME detector is given.

(2) The robustness of MME detector with the uncertainty of the transmitter-target and receiver-target distances in SCFNR is analyzed. Using the channel gain matrix in one coherent pulse interval (CPI), the closed-form of the lower bound of the test statistic under the presence of target return, and the upper bound under the absence of target return are given respectively.

(3) Using the mobility model about transmitter- receiver pairs in SCFNR, we derive the interval between the upper bound of transmitter-receiver distance and the lower bound in SCFNR for robust MME detection. Then we give the constraint on the bounded relative distance for robust MME detector in SCFNR. We validate the effectiveness of the proposed constraint through numerical calculations also.

The rest of the paper is organized as follows: Section II reviews the system model for the robust MME detection problem caused by the uncertainty of geometric configuration in SCFNR, including the mobility model for bistatic radar pair, signal model, channel gain matrix, the definition of robust detector, etc. Section III focuses on the detecting robustness due to the uncertainty of geometric configuration in SCFNR. Section IV verifies the effectiveness of the proposed robust MME detector with numerical calculations. Finally, we conclude the paper in Section V.

II. THE SYSTEM MODEL

Generally, netted radar has the following three cases: a group of bistatic radars, a single transmitter with several receivers, and a single receiver with several transmitters [12]. In this paper, we adopt SCFNR with bistatic radar pairs. It is assumed that one-to-one pairing method is taken by SCFNR in any slot of the orbital hyper-period [22]. So, we assume that each pair of transmitter and receiver can potentially form a bistatic radar. We further assume that orthogonal transmissions are used for interference avoidance. In view of this, we assume that one transmitter can only be connected to one receiver, and the corresponding bistatic radar is formed in any slot of the orbital hyper-period [12], [22].

In this paper, we focus on the robust MME detection problem caused by the uncertainty of the geometric configuration in SCFNR. The uncertainty of the geometric configuration is caused by the mobility model of the transmitter-receiver pair in SCFNR. Therefore, it is necessary to analyze the mobility model of SCFNR and describe the signal model in SCNR first.

A. THE MOBILITY MODEL FOR BISTATIC RADAR PAIR

To accomplish the cluster flight model within bounded distance, the twin-satellites model is adopted to study the mobility model for bistatic radar pair. As shown in Figure 1, the transmitter or receiver position is uniformly distributed on sphere within $R = (M - m)/4$. M is the upper bound of transmitter-receiver distance in SCFNR, and m is the lower bound.

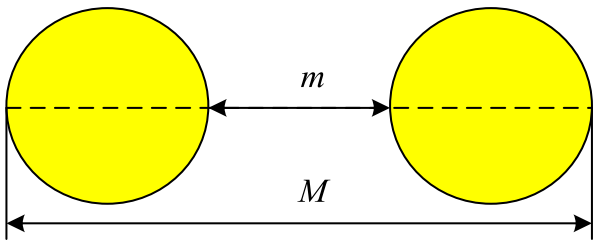

FIGURE 1. The mobility model for bistatic radar pair.

Based on orbit dynamics theory, the orbital hyper-period can be divided into $(t_0, t_1, \cdots, t_T)$ times for fractionated spacecraft [2], [23]. So, there are T time slots in one orbital period. The orbital hyper-period is $H = (t_T - t_0)$, $\sigma_k = [t_{k-1}, t_k)$, $(k = 1, 2, \cdots, N)$. So, the mobility model M(t) for bistatic radar pair can be defined as follows:

Definition 1: In Earth-centered inertial (ECI) coordinates, if the position set of N transmitter-receiver pairs in SCFNR is $S(0) = \{S_1(0), S_2(0), \ldots, S_N(0)\}$ at initial time t_0, the position set is $\boldsymbol{S}(k) = \{S_1(k), S_2(k), \ldots, S_N(k)\}$ at time t_k, and the positions are uniformly distributed within sphere $B(S_p(0), R)$, $(p = 1, 2, \ldots, N)$, where $S_p(0)$ and $R = (M - m)/4$ are center and radius of the sphere respectively. Moreover, positions among all transmitters and receivers

are mutually independent and independent of all previous locations.

B. SIGNAL MODEL

Considering the SCFNR scenario as shown in Figure 2. Let $\boldsymbol{T}$ be the transmitter set, $\boldsymbol{R}$ be the receiver set. The transmitters and receivers are located at different locations. We use $\boldsymbol{TR}$ to denote all transmitter-receiver pairs. If transmitter $T_p \in \boldsymbol{T}$ and receiver $R_q \in \boldsymbol{R}$ select the same channel, then the bistatic radar $T_pR_q \in \boldsymbol{TR}$ is formed by T_p and $R_q(p, q = 1, 2, \cdots, N)$. And different channels can be considered as orthorhombic channels to avoid interference. Without ambiguity, in any time slot of orbital hyper-period for SCFNR, the positions of transmitter and receiver are denoted by S_{pT} and S_{qR} respectively.

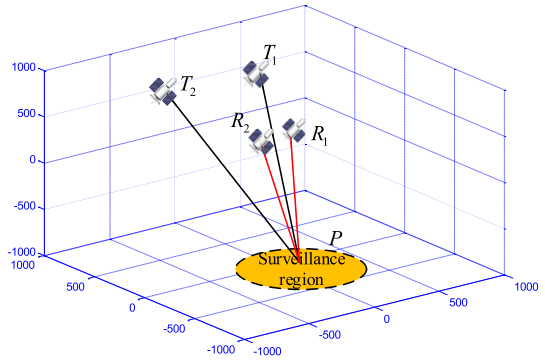

FIGURE 2. The SCFNR scenario.

Considering the i^{th} bistatic radar of SCFNR to transmit L pulses in one CPI, and the received data forms an L-dimensional vector is called a snapshot after sampling. The snapshot can be given as:

$$\boldsymbol{x_i} = [x_i(0), x_i(1), \cdots, x_i(L-1)]^H \tag{1}$$

where the subscript H denotes the complex conjugate.

So, for target detection of bistatic radar, two scenarios are considered as follows:

Hypothesize $\mathcal{H}_1$: $\mathcal{H}_1$ denotes the presence of the target, and the sample outputs $\mathbf{x_i}$ at the receiver can be represented as follows:

$$\boldsymbol{x_i} = \boldsymbol{G_i s_i} + \boldsymbol{u_i} \tag{2}$$

where $\boldsymbol{u_i} = [u_i(0), u_i(1), \cdots, u_i(L-1)]^{\mathrm{H}}$ is a $L \times 1$ disturbance vector, $\boldsymbol{s_i} = [s_i(0), s_i(1), \cdots, s_i(L-1)]^{\mathrm{H}}$ is a $L \times 1$ transmitted signal vector, $\boldsymbol{G}$ is a $L \times L$ channel matrix from transmitter to receivers.

Hypothesize $\mathcal{H}_0$: $\mathcal{H}_0$ denotes the absence of the target, and the sample outputs $\mathbf{x_i}$ at the receivers can be represented as follows:

$$\boldsymbol{x_i} = \boldsymbol{u_i} \tag{3}$$

For convenience, we make the following assumptions for the above scenarios.

1) The disturbances vector $\boldsymbol{u_i}$ is distributed according to circularly symmetric complex Gaussian noise with zero mean and variance σ_u^2, i.e., $\boldsymbol{u}_i \sim \mathcal{CN}\left(0, \sigma_u^2\right)$.

2) The power of transmitted pulse signal of radar is assumed to be σ_s^2.

3) $\boldsymbol{s_i}$ and $\mathbf{u_i}$ are independent of each other.

Considering the fact that both the signal and the disturbance are zero-mean, the statistical covariance matrices can be obtained as

$$\begin{aligned}
\mathbf{R}_{si} &= \mathbb{E}\left[\mathbf{s}_i\mathbf{s}_i^{\mathrm{H}}\right] \\
\mathbf{R}_{ui} &= \mathbb{E}\left[\mathbf{u}_i\mathbf{u}_i^{\mathrm{H}}\right] \\
\mathbf{R}_{xi} &= \mathbb{E}\left[\mathbf{x}_i\mathbf{x}_i^{\mathrm{H}}\right] = \mathbf{G}_i\mathbf{R}_{si}\mathbf{G}_i^{\mathrm{H}} + \mathbf{R}_{ui}
\end{aligned} \tag{4}$$

Due to the small sample interval in the CPI, for convenience, it can be assumed that the Doppler shift of each sample is the same. Based on this, in the CPI, the autocorrelation function of the transmitted signal can be given by (5):

$$\begin{aligned}
R_{ii}(k) &= \frac{1}{2T}\int_{-T}^{T}\left[s_i(t)s_i(t \pm k)\right]dt \\
&\approx \begin{cases} \sigma_s^2\left(1 - \dfrac{k}{L}\right), & \text{if } |k| \le L \\ 0, & \text{else}, \quad k = 0, 1, \cdots, L-1 \end{cases}
\end{aligned} \tag{5}$$

where T is the period of the pulse signal.

So, the covariance matrix $\mathbf{R}_{si}$ can be expressed as:

$$\mathbf{R}_{\mathrm{si}} = \sigma_s^2\begin{bmatrix} 1 & \frac{L-1}{L} & \cdots & \frac{1}{L} \\ \frac{L-1}{L} & 1 & \cdots & \frac{2}{L} \\ \vdots & \vdots & \ddots & \vdots \\ \frac{1}{L} & \frac{2}{L} & \cdots & 1 \end{bmatrix} \tag{6}$$

Then, for N pairs of bistatic radars in SCFNR, $\boldsymbol{x}$, $\boldsymbol{s}$ and $\boldsymbol{u}$ are expressed respectively as:

$$\begin{aligned}
\boldsymbol{x} &= [\boldsymbol{x_1}, \boldsymbol{x_2}, \cdots, \boldsymbol{x}_N]^{\mathrm{H}} \\
\boldsymbol{s} &= [\boldsymbol{s_1}, \boldsymbol{s_2}, \cdots, \boldsymbol{s}_N]^{\mathrm{H}} \\
\boldsymbol{u} &= [\boldsymbol{u_1}, \boldsymbol{u_2}, \cdots, \boldsymbol{u}_N]^{\mathrm{H}}
\end{aligned} \tag{7}$$

Since $\boldsymbol{x_i}$ and $\boldsymbol{u_i}(i = 1, 2, \cdots, N)$ of different bistatic radars are independent and identically distributed in both spatially and temporally, $\boldsymbol{x}$ has a $N \times L$ dimensional joint complex Gaussian distribution that can be expressed as

$$x = \begin{cases} \mathcal{CN}\left(\mathbf{0}, \sigma_u^2\mathbf{I}\right), & \Rightarrow \mathcal{H}_0 \\ \mathcal{CN}\left(\mathbf{0}, \mathbf{G}\mathbf{R}_{\mathrm{s}}\mathbf{G}^{\mathrm{H}} + \sigma_u^2\mathbf{I}\right), & \Rightarrow \mathcal{H}_1 \end{cases} \tag{8}$$

The received signal vector $\boldsymbol{x}$ obeys the complex Gaussian distribution with the covariance matrices $\mathbf{R}_x^0$ and $\mathbf{R}_x^1$ at the hypotheses $\mathcal{H}_0$ and $\mathcal{H}_1$, respectively. The covariance matrices $\mathbf{R}_x^0$ and $\mathbf{R}_x^1$ can be expressed as:

$$\begin{aligned}
\mathbf{R}_x^0 &= \mathbb{E}\left[\boldsymbol{x}\boldsymbol{x}^{\mathrm{H}} \mid \mathcal{H}_0\right] = \sigma_u^2\mathbf{I} \\
\mathbf{R}_x^1 &= \mathbb{E}\left[\boldsymbol{x}\boldsymbol{x}^{\mathrm{H}} \mid \mathcal{H}_1\right] = \boldsymbol{\mathcal{G}} + \sigma_u^2\mathbf{I}
\end{aligned} \tag{9}$$

where $\boldsymbol{\mathcal{G}} = \mathbf{G}\mathbf{R}_{\mathrm{s}}\mathbf{G}^{\mathrm{H}}$.

C. CHANEL GAIN MATRIX

The Eq. (9) shows that the sample covariance matrix $\mathbf{R}_x^1$ is determined by channel gain matrix $\mathbf{G}$ if keeping $\mathbf{R}_s$ and σ_u^2 fixed. And the entries of $\mathbf{G}$ are modeled by the target amplitude times. Furthermore, the independence of the snapshots from different bistatic radars also implies that $\mathcal{G}$ has a block-diagonal structure as follows:

$$\mathcal{G} = \begin{bmatrix} \mathcal{G}_1 & & \mathbf{0} \\ & \mathcal{G}_2 & \\ & \ddots & \\ \mathbf{0} & & \mathcal{G}_N \end{bmatrix}_{LN \times LN} \tag{10}$$

$\mathcal{G}_i$ $(i = 1, 2, \cdots, N)$ is a symmetric matrix due to the correlations between pules in the CPI. If the correlations are not considered, $\mathcal{G}_i$ is a diagonal matrix, and the diagonal entry of $\mathcal{G}_i$ represents the power transforming coefficient in accordance with the target reflectivity, the antenna gain, and the channel propagation effects of the bistatic radar.

For $T_pR_q \in \boldsymbol{TR}$ in SCFNR, the received power at the receiver R_q is given as follows [25]:

$$P_{pq} = \frac{P_T K_B}{\left\|S_{pT}P\right\|^2 \left\|PS_{qR}\right\|^2} \tag{11}$$

where $K_B = G_T G_R \sigma \lambda^2/(4\pi)^3$, P_T is the peak power of the radar transmitted signal, σ is the radar cross-section, G_T and G_R are the gain of the transmitting and receiving antenna respectively, $\left\|S_{pT}P\right\|$ and $\left\|PS_{qR}\right\|$ denote transmitter-target and target-receiver distances, respectively. However, we are not interested in the SCFNR physical-layer parameters, but in transmitter-target and target-receiver distances. For convenience, we assume that the constant is identical for any bistatic radar, i.e., homogeneous bistatic radar also.

In the CPI, let $d_p(s) = \left\|S_{pT}P\right\|$ and $d_q(t) = \left\|PS_{qR}\right\|$ $(s, t = 0, 1. \cdots, L-1)$ denote transmitter-target distance at time s and target-receiver distance at time t respectively. Then using (11), for the i^{th} bistatic radars, the gain matrix $\mathbf{G}_i$ is denoted by (12):

$$\mathbf{G}_i = \sqrt{K_B} diag\left(\frac{1}{\left\|d_p(0)\right\| \left\|d_q(0)\right\|}, \cdots, \frac{1}{\left\|d_p(L-1)\right\| \left\|d_q(L-1)\right\|}\right) \tag{12}$$

And substituting (6) and (12) into $\mathcal{G} = \mathbf{G}\mathbf{R}_s\mathbf{G}^H$, we get (13).

$$\mathcal{G}_i = \mathbf{G}_i \mathbf{R}_{si} \mathbf{G}_i^H = K_B \sigma_s^2 \left(a_{ij}\right)_{L \times L} \tag{13}$$

where

$$a_{ij} = a_{ji} = \frac{L + (i-j)}{L} d_{ij},$$
$$d_{ij} = \frac{1}{\left\|d_p(i-1)\right\| \left\|d_q(i-1)\right\| \left\|d_p(j-1)\right\| \left\|d_q(j-1)\right\|}, \quad 1 \le i \le j \le L.$$

This means that the target detection performance depends on the geometric configuration in SCFNR. And we can substitute the uncertainty set d_{ij} for uncertainty of geometric configuration.

D. ROBUST DETECTOR IN SCFNR

According to section II.C, it is known that the target detection performance depends on the geometric configuration in SCFNR. However, the high-speed flight of platform increases the uncertainty of geometric configuration in SCFNR, which makes the product of transmitter-target and target-receiver distances d_{pq} uncertain. So, how to evaluate the robustness of target detection is critical in SCFNR. And this paper is addressed to analyze the robustness caused by this uncertainty of geometric configuration in SCFNR.

In this paper, we apply MME detection to the target detection in SCFNR, and the test statistics is composed of the eigenvalues of the received signal's sample covariance matrix $\mathbf{R}_x$ at fusion center. The test statistic and its accompanying decision rule in the mobility model M(t) are given by

$$\Gamma_{MME}\left(\boldsymbol{x}, M(t)\right) = \frac{\lambda_{\max}\left(\mathbf{R}_x\right)}{\lambda_{\min}\left(\mathbf{R}_x\right)} \underset{\mathcal{H}_\infty}{\overset{\mathcal{H}_\prime}{\lessgtr}} \gamma \tag{14}$$

where $\lambda_{\max}\left(\mathbf{R}_x\right)$ and $\lambda_{\min}\left(\mathbf{R}_x\right)$ denote the largest and smallest eigenvalue of the matrix $\mathbf{R}_x$, respectively. γ stands for the predefined decision threshold, and M(t) represents the mobile model in Definition 1.

For SCFNR, the probability of false alarm and the probability of missed detection due to the uncertainty of geometric configuration can be defined as:

$$\begin{aligned} P_{fa}\left(\mathrm{M}(t)\right) &= P\left(\Gamma_{\mathrm{MME}}\left(\boldsymbol{x}, M(t)\right) \ge \gamma \,|\mathcal{H}_0, \mathrm{M}(t)\right) \\ P_{md}\left(\mathrm{M}(t)\right) &= P\left(\Gamma_{\mathrm{MME}}\left(\boldsymbol{x}, M(t)\right) < \gamma \,|\mathcal{H}_1, \mathrm{M}(t)\right) \end{aligned} \tag{15}$$

However, for SCNFR, the uncertainty of the geometric configuration in SCFNR due to the mobility of the transmitter and receiver further leads to the problem of robust target detection. Inspired by [24], we can define whether the detector is robust by a pair (P_{fa}, P_{md}) consisting of a target false alarm probability P_{fa} and a target missed detection probability P_{md} if it satisfies

$$\begin{cases} P_{fa}(\mathrm{M}(t)) < 0.5 \\ P_{md}(\mathrm{M}(t)) < 0.5 \end{cases} \tag{16}$$

So, we can define the robust detector for the uncertainty of geometric configuration in SCFNR as follows:

Definition 2: A detector is called robust in SCFNR, if the false-alarm and missed-detection probabilities are both smaller than 1/2.

For $\mathcal{H}_1$ and $\mathcal{H}_0$ test statistics, if there is a $\mathcal{H}_0$ mean that is below one of the $\mathcal{H}_1$ means, no matter what value is chosen for the threshold, either $P_{fa}(\mathrm{M}(t))$ or $P_{md}(\mathrm{M}(t))$ is always less than 0.5 [15]. So, we can find a lower bound $\bar{\Gamma}^{\mathrm{lo}}_{\mathrm{MME},\mathcal{H}_1}$ on the test statistic $\Gamma_{\mathrm{MME}}(\boldsymbol{x}, \mathrm{M(t)})$ under $\mathcal{H}_1$ and an upper bound $\bar{\Gamma}^{\mathrm{up}}_{\mathrm{MME},\mathcal{H}_0}$ under $\mathcal{H}_0$ respectively. If $\bar{\Gamma}^{\mathrm{lo}}_{\mathrm{MME},\mathcal{H}_1} \ge \bar{\Gamma}^{\mathrm{up}}_{\mathrm{MME},\mathcal{H}_0}$,

the MME detector is robust. Bounds are denoted by a bar above the respective symbol.

III. ROBUST ANALYSIS FOR MME DETECTION IN SCFNR

In this section, we analyze the robustness of MME detector with the uncertainty of geometric configuration in SCFNR, thus proving its existence. In (9), $\mathbf{R}_x = \mathbf{G}\mathbf{R}_s\mathbf{G}^{\mathrm{H}} + \sigma_u^2\mathbf{I} = \boldsymbol{\mathcal{G}} + \mathbf{R}_u$, the matrices $\boldsymbol{\mathcal{G}}$ and $\mathbf{R}_u$ are Toeplitz matrices. The disturbance vector $\mathbf{u}$ is distributed according to a circularly symmetric complex Gaussian distribution, i.e., $\mathbf{u} \sim \mathcal{CN}\left(0, \sigma_u^2\right)$.

A. THE TRANSMITTER-TARGET AND TARGET-RECEIVER DISTANCES

The 2D Cartesian coordinate system in SCFNR is established with the target as the origin in Figure 3. Let the positions of transmitter and receiver for a bistatic radar $T_pR_q \in \boldsymbol{TR}$ be (x_p, y_p) and (x_q, y_q) at initial time T_0 respectively. And the slopes from the origin to (x_p, y_p) and (x_q, y_q) are k_p and k_q correspondingly. The distances between (x_0, y_0) and (x_p, y_p), (x_0, y_0) and (x_q, y_q) are $C_p = \left|x_p\sqrt{1+k_p^2}\right|$ and $C_q = \left|x_q\sqrt{1+k_q^2}\right|$, respectively. So, the largest and smallest distances between the transmitter and target in the mobile model M(t) are given as follows:

$$\begin{cases} d_p^{\max} = C_p + \dfrac{M-m}{4} \\ d_p^{\min} = C_p - \dfrac{M-m}{4} \end{cases} \tag{17}$$

Similarly, the largest and smallest distances between the receiver and target in the mobile model $\bar{\Gamma}_{MME,\mathcal{H}_1}^{lo}$ are given as follows:

$$\begin{cases} d_q^{\max} = C_q + \dfrac{M-m}{4} \\ d_q^{\min} = C_q - \dfrac{M-m}{4} \end{cases} \tag{18}$$

B. THE LOWER BOUND $\bar{\Gamma}_{MME,\mathcal{H}_1}^{lo}$ AND THE UPPER BOUND $\bar{\Gamma}_{MME,\mathcal{H}_0}^{up}$

In order to analyze the robustness of MME detector in SCFNR, the lower bound $\bar{\Gamma}_{\mathrm{MME},\mathcal{H}_1}^{\mathrm{lo}}$ and the upper bound $\bar{\Gamma}_{\mathrm{MME},\mathcal{H}_0}^{\mathrm{up}}$ need to be calculated.

Case 1: The lower bound $\bar{\Gamma}_{\mathrm{MME},\mathcal{H}_1}^{\mathrm{lo}}$ under $\mathcal{H}_1$

Let $\lambda_{\max}(\cdot)$ and $\lambda_{\min}(\cdot)$ denote the largest and smallest eigenvalue of a matrix respectively. And the lower bound $\bar{\Gamma}_{\mathrm{MME},\mathcal{H}_1}^{\mathrm{lo}}$ on the asymptotic test statistic can be given as follows:

$$\frac{\bar{\lambda}_{\max}^{\mathrm{lo}}(\mathbf{R}_x)}{\bar{\lambda}_{\min}^{\mathrm{up}}(\mathbf{R}_x)} = \bar{\Gamma}_{\mathrm{MME},\mathcal{H}_1}^{\mathrm{lo}} \le \Gamma_{\mathrm{MME},\mathcal{H}_1} = \frac{\lambda_{\max}(\mathbf{R}_x)}{\lambda_{\min}(\mathbf{R}_x)} \tag{19}$$

To obtain the lower bound $\bar{\Gamma}_{\mathrm{MME},\mathcal{H}_1}^{\mathrm{lo}}$, we need to determine a lower bound on the largest eigenvalue $\bar{\lambda}_{\max}^{\mathrm{lo}}(\mathbf{R}_x)$ and an upper bound on the smallest eigenvalue $\bar{\lambda}_{\min}^{\mathrm{up}}(\mathbf{R}_x)$:

$$\begin{cases} \bar{\lambda}_{\max}^{\mathrm{lo}}(\mathbf{R}_x) \le \lambda_{\max}(\mathbf{R}_x) \\ \bar{\lambda}_{\min}^{\mathrm{up}}(\mathbf{R}_x) \ge \lambda_{\min}(\mathbf{R}_x) \end{cases} \tag{20}$$

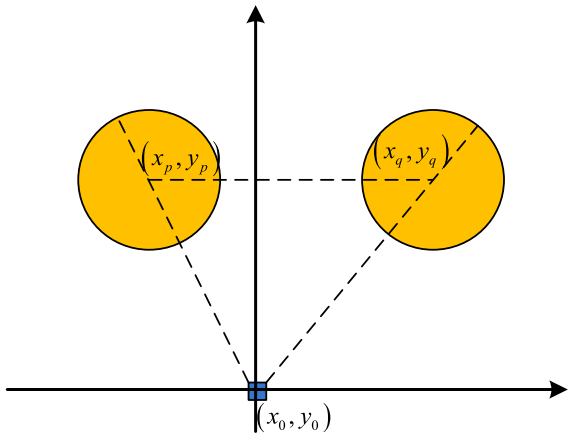

FIGURE 3. The 2D Cartesian coordinate system in SCFNR.

Without loss of generality, we assume that the largest correlation coefficient is located at the k^{th} column of the first row of the matrix $\mathbf{R}_x$ and the i^{th} block-matrix. According to the Courant-Fischer theorem, we can obtain (21) [15].

$$\begin{cases} \bar{\lambda}_{\max^{\mathrm{lo}}}(\mathbf{R}_x) = \sigma_u^2 + K_B\sigma_s^2/d_{11} + \rho_k K_B\sigma_s^2/d_{1,k+1} \\ \bar{\lambda}_{\max^{\mathrm{up}}}(\mathbf{R}_x) = \sigma_u^2 + K_B\sigma_s^2/d_{11} - \rho_k K_B\sigma_s^2/d_{1,k+1} \end{cases} \tag{21}$$

where

$$\rho_k = 1 - k/L,$$
$$d_{ij} = \frac{1}{\left\|d_p(i-1)\right\|\left\|d_q(i-1)\right\|\left\|d_p(j-1)\right\|\left\|d_q(j-1)\right\|}.$$

Hence, the lower bound $\Gamma_{\mathrm{MME},\mathcal{H}_1}^{\mathrm{lo}}$ under $\mathcal{H}_1$ is now given by

$$\Gamma_{\mathrm{MME},\mathcal{H}_0}^{\mathrm{lo}} = \frac{\sigma_u^2 + K_B\sigma_s^2/d_{11} + \rho_k K_B\sigma_s^2/d_{1,k+1}}{\sigma_u^2 + K_B\sigma_s^2/d_{11} - \rho_k K_B\sigma_s^2/d_{1,k+1}} \tag{22}$$

Case 2: The l upper bound $\bar{\Gamma}_{\mathrm{MME},\mathcal{H}_0}^{\mathrm{up}}$ under $\mathcal{H}_0$

For this case, the upper bound $\bar{\Gamma}_{\mathrm{MME},\mathcal{H}_0}^{\mathrm{up}}$ on the test statistic is given as follows:

$$\frac{\bar{\lambda}_{\max}^{\mathrm{up}}(\mathbf{R}_x)}{\bar{\lambda}_{\min}^{\mathrm{lo}}(\mathbf{R}_x)} = \bar{\Gamma}_{\mathrm{MME},\mathcal{H}_0}^{\mathrm{up}} \ge \Gamma_{\mathrm{MME},\mathcal{H}_0} = \frac{\lambda_{\max}(\mathbf{R}_x)}{\lambda_{\min}(\mathbf{R}_x)} \tag{23}$$

According to the Gershgorin circle theorem, an upper bound on the maximum eigenvalue of $\mathbf{R}_x$ can be obtained as [15]

$$\bar{\lambda}_{\max}^{\mathrm{up}}(\mathbf{R}_x) = \sigma_s^2 = \lambda_{\max}(\mathbf{R}_x) \tag{24}$$

And a lower bound on the minimum eigenvalue of $\frac{\sigma_u^2 + K_B\sigma_s^2/d_{11} + \rho_k K_B\sigma_s^2/d_{1,k+1}}{\sigma_u^2 + K_B\sigma_s^2/d_{11} - \rho_k K_B\sigma_s^2/d_{1,k+1}} \ge 1$ can be obtained as

$$\bar{\lambda}_{\min}^{\mathrm{lo}}(\mathbf{R}_x) = \sigma_u^2 = \lambda_{\min}(\mathbf{R}_x) \tag{25}$$

So, the upper bound $\bar{\Gamma}_{\mathrm{MME},\mathcal{H}_0}^{\mathrm{up}}$ under $\mathcal{H}_0$ is 1.

Hence, the MME detector is robust when $\bar{\Gamma}_{\mathrm{MME},\mathcal{H}_1}^{\mathrm{lo}} \ge \bar{\Gamma}_{\mathrm{MME},\mathcal{H}_0}^{\mathrm{up}}$, i.e. (26),

$$\frac{\sigma_u^2 + K_B\sigma_s^2/d_{11} + \rho_k K_B\sigma_s^2/d_{1,k+1}}{\sigma_u^2 + K_B\sigma_s^2/d_{11} - \rho_k K_B\sigma_s^2/d_{1,k+1}} \ge 1 \tag{26}$$

In (26), we make sure that $\bar{\lambda}_{\min}^{\text{up}}(\mathbf{R}_x) > 0$, which leads to the constrained (27):

$$\sigma_u^2 + K_B\sigma_s^2/d_{11} - \rho_k K_B\sigma_s^2/d_{1,k+1} > 0 \tag{27}$$

C. CONSTRAINT ON BOUNDED RELATIVE DISTANCE FOR ROBUST MME DETECTION

In the absence of control, the two initially closed transmitter and receiver platforms rapidly separate due to different accelerations. It is thus necessary to identify orbits on which the transmitter and receiver platforms remain within some pre-specified relative distance for the entire mission lifetime in SCFNR [2]. Also, it needs to identify orbits for robust MME detecting in SCFNR.

The orbits of all transmitter and receiver platforms are determined by Earth-centered inertial (ECI) coordinate system. ECI is defined in the following standard manner [2]: the fundamental plane is the equatorial plane; the $\mathbf{x}$ axis towards the vernal equinox, the $\mathbf{z}$ axis points towards the geographic north pole, and $\mathbf{y} = \mathbf{z} \times \mathbf{x}$. The vector of classical orbital elements in ECI coordinate, which describes natural orbits of fractionated spacecraft, is defined as:

$$\boldsymbol{\alpha} \triangleq [a, e, \beta, \omega, f, \Omega]^{\mathrm{T}} \tag{28}$$

where a is the semimajor axis, e is the eccentricity, β is the inclination, ω is the argument of perigee, f is the true anomaly, and Ω is the right ascension of ascending node (RAAN).

If the vector $\mathbf{r} = [x, y, z]^T$ denotes the position of any satellites in FSN in ECI coordinate, $\mathbf{v} = d\mathbf{r}/dt$ is the velocity, $\eta = \sqrt{x^2 + y^2}$ is equatorial projection of position vector, as well as the maximal and minimal equatorial projections of the position vector of satellite at time t, given by $\eta_{\max} = \max_t \eta(t)$ and $\eta_{\min} = \min_t \eta(t)$, where $\eta(t) = \sqrt{x^2(t) + y^2(t)}$.

To obtain the initial constraint to SCFNR with respect to keep bounded relative distance, the proposition is given as following [2]:

Proposition: Consider two modules, the transmitter platform C and the receiver platform D, having identical constant ballistic coefficients, i.e.,

$$\frac{C_{D_C} S_C}{m_C} = \frac{C_{D_D} S_D}{m_D} = \text{cons} \tag{29}$$

where S is the cross-sectional area, C_D is the drag coefficient defined with respect to the cross-sectional area, m_C and m_D are the mass of the transmitter platform C and the receiver platform D, respectively. In the following development, the subscripts $(.)_C$ and $(.)_D$ denote quantities corresponding to the satellites C and D, respectively. If only the atmospheric drag and the zonal harmonics with gravitational potential are considered, satellite D requires initial conditions to be satisfied as follows:

$$\alpha_D(t_0) = \alpha_C(t_0) + \int_{t_0}^{t_0+\Delta t} \dot{\alpha}_A dt + \begin{bmatrix} \mathbf{0}_{5\times 1} \\ \Delta\Omega \end{bmatrix} \tag{30}$$

where $\mathbf{0}_{5\times 1}$ denotes a five-dimensional-zeros vector, differential RAAN satisfy

$$\Delta\Omega = \Omega_D(t_0) - \Omega_C(t_0 + \Delta t) \tag{31}$$

And the distance between the transmitter platform C and the receiver platform D is required to satisfy (32).

$$\begin{aligned} &2\eta_{\min} \sin\left(\frac{|\Delta\Omega|}{2}\right) - |\Delta t|\, v_{\max} \\ &\le |\mathbf{r}_D(t) - \mathbf{r}_C(t)| \\ &\le 2\eta_{\max} \sin\left(\frac{|\Delta\Omega|}{2}\right) + |\Delta t|\, v_{\max} \end{aligned} \tag{32}$$

Eq. (32) gives the bound of relative distance between the transmitter platform and the receiver platform. For robust MME detecting, we need to analyze the constraints on the relative distances.

We give related theorems 1 and 2, and their proofs are shown in the appendix.

Theorem 1: If the chief module C and the deputy module D of SCFNR have identical constant ballistic coefficients, if $\frac{\eta_{\max} - \eta_{\min}}{v_{\max}} \le \frac{\sin(|\Delta\Omega|/2)}{|\Delta t|}$, the difference between M and m satisfy (33).

$$\begin{aligned} 2v_{\min}|\Delta t| &\le M - m \\ &\le 2\eta_{\max} \sin\left(\frac{|\Delta\Omega|}{2}\right) - 2\eta_{\min} \sin\left(\frac{|\Delta\Omega|}{2}\right) \\ &\quad + 2v_{\max}|\Delta t| \end{aligned} \tag{33}$$

Theorem 2: In SCFNR, if the initial position of transmitter $S_{iT}(0)$ and mobility model $\mathrm{M}(t)$ are given, let $d_t^{\max} = \min\{d_p^{\max}\}, d_r^{\max} = \min\{d_q^{\max}\}$ and $d_t^{\min} = \min\{d_p^{\min}\}, d_r^{\min} = \min\{d_q^{\min}\}$, the MME detector is robust under the condition given by (29) when

$$0 < M - m \le 2 \cdot \frac{-b + \sqrt{b^2 - 4ac}}{a},$$

where

$$\begin{aligned} &C = \max\{C_p, C_q\}, \quad D = \min\{C_p, C_q\}, \\ &a = \frac{20K_B\sigma_s^2\rho_k}{D^6} - \frac{20K_B\sigma_s^2}{C^6}, \quad b = \frac{4K_B\sigma_s^2\rho_k}{D^5} + \frac{4K_B\sigma_s^2}{C^5}, \\ &c = \frac{K_B\sigma_s^2\rho_k}{D^4} - \frac{K_B\sigma_s^2}{C^4} - \sigma_u^2. \end{aligned}$$

Thus, to identify orbit elements on which the transmitter and receiver platforms remain within some pre-specified relative distance for the entire mission lifetime in SCFNR, and to identify orbit elements for robust MME detecting in SCFNR, the corollary is as follows:

Corollary: Given M - m, the condition of orbit elements (maximum distance difference) for robust MME detector in the entire mission lifetime of SCFNR must be satisfied:

$$2v_{\min}|\Delta t| \le M - m \le \Phi \tag{34}$$

where

$$\Phi = \min\left\{2\eta_{\max} \sin\left(\frac{|\Delta\Omega|}{2}\right) - 2\eta_{\min} \sin\left(\frac{|\Delta\Omega|}{2}\right)\right.$$

TABLE 1. All near circular orbital elements of SCFNR.

Parameter	Semimajor axis (km)	Eccentricity (deg)	Inclination (deg)	Argument of perigee (deg)	True anomaly (deg)	Right ascension of ascending node (deg)
T_1	7378.14	0.02	35	0	0	0
T_2	7378.14	0.02	35	0.00163	1.13947	3.3882
T_3	7378.14	0.02	35	0.00068	0.47630	1.82400
T_4	7378.14	0.02	35	359.997	-2.1650	1.70983
R_1	7378.14	0.02	35	0.00106	2.50602	2.50602
R_2	7378.14	0.02	35	0.00022	0.15383	1.08022
R_3	7378.14	0.02	35	359.999	-0.79763	4.02245
R_4	7378.14	0.02	35	0.00344	2.39289	-1.18115

TABLE 2. Parameter setting.

Parameter	Value	Parameter	Value
K_B	$45M^4$	σ_u^2	0.005 dBW
L	2,3,4	γ	2
σ_s^2	5 dBW	N	4

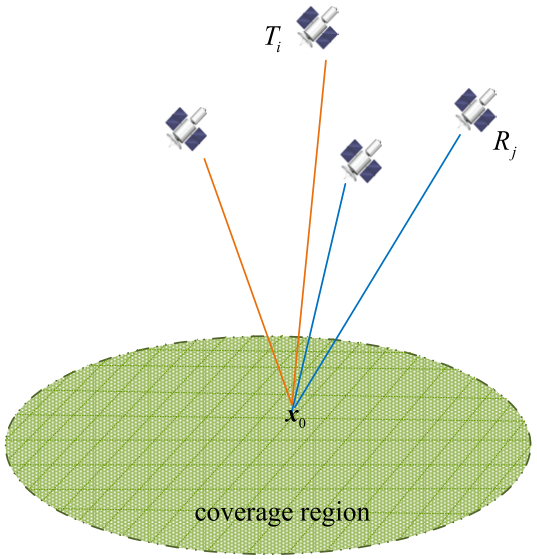

FIGURE 4. Simulation scenario in SCFNR.

$$+2v_{\max}|\Delta t|, \frac{-2b+2\sqrt{b^2-4ac}}{a}\Bigg\}.$$

IV. NUMERICAL CALCULATION

In order to simulate and analyze the robustness of MME detector for SCFNR in time slot of the orbital hyper-period, we need to establish the SCFNR scenario by STK (Satellite Tool Kit) in Figure 4. And we fulfil numerical simulation in Windows 10 and MATLAB R2017b environment.

A. PARAMETER SETTINGS

Suppose SCFNR is composed of 4 pairs of homogeneous bistatic radars. Let $\boldsymbol{T} = \{T_1, T_2, T_3, T_4\}$, $\boldsymbol{R} = \{R_1, R_2, R_3, R_4\}$, $m = 30$ km, $M = 580$ km. According to the orbit design of cluster flight spacecraft proposed in using (34), all near circular orbital elements of SCFNR are listed in Table 1. And the other parameter settings are listed in Table 2.

B. TRANSMITTED POWER'S EFFECT ON THE BOUND OF RELATIVE DISTANCE

According to Table 1, all orbital periods can be calculated and are approximated as 6310 seconds using STK. So, we believe the orbital hyper-periods of the SCFNR are also 6310 s. In addition, as shown in Figure 5, we can also calculate all relative distances between transmitters and receivers in 172 days by STK. For convenience, the CPI is taken as the width of time slot in orbital hyper-period. Considering the number L of pulse in a CPI is 2, 3 and 4 respectively, then $\rho_k = 1/2, 2/3$ and 3/4 in (21) correspondingly. And let $B = \frac{-2b+2\sqrt{b^2-4ac}}{a}$, the transmitted power's effect on the bound of relative distance in SCFNR can be shown in Figure 6.

And the relation between the transmitted power and $\bar{\Gamma}^{\text{lo}}_{\text{MME},\mathcal{H}_1}$ is shown in Figure 7(a)-(c) correspondingly.

In Figure 7, the results can be analyzed as follows:

(1) It is observed that all up bound of R is greater than 205 km, irrespective of ρ_k. And it shows that the MME detector in SCFNR is robust in Figure 5. This satisfies the constraint in Theorem 2. So, designing the orbit of SCFNR can ensure the relative distances bounded and the MME detector robust.

(2) It is observed that $\bar{\Gamma}_{\text{MME}}$ is greater than 1 in Figure 6-8, and the MME detector is robust according to (26) irrespective of ρ_k. The results are consistent with the above. Also, the Γ_{MME} increases with the ρ_k increasing.

(3) In Figure 7(a)-(c), the up bound of R approaches some constant, and the Γ_{MME} approaches some constant too.

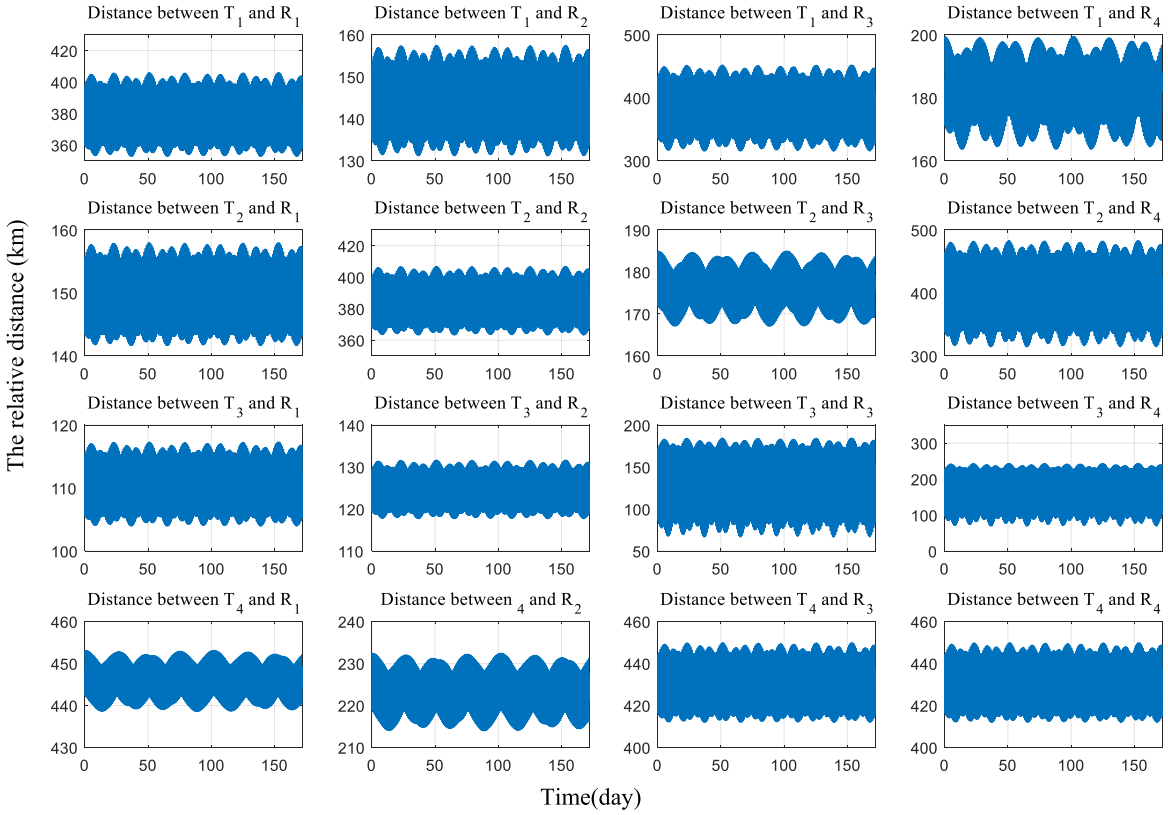

FIGURE 5. The relative distance between any transmitter-receiver within 172 days.

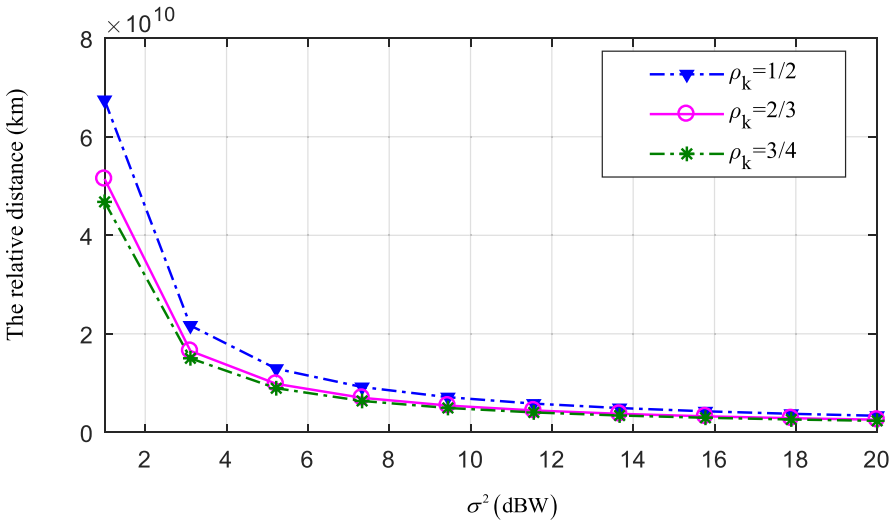

FIGURE 6. The transmitted power's effect on the bound of relative distance in SCFNR.

All approaching trends are the same. The reason is that the higher the transmitted power, the more negligible the other factors in (22) are.

C. FALSE-ALARM PROBABILITY AND MISSED-DETECTION PROBABILITY

Using the method in [26], the false-alarm probability and the missed-detection probability can be calculated. So, the relation between the transmitted power and the false-alarm probability, the missed-detection probability is shown in Figure 8 while $\rho_k = 1/2$, 2/3, and 3/4 respectively.

In Figure 8, both the false-alarm probability and the missed-detection probability are smaller than 0.5. According to Definition 2, the MME detector is robust. This is consistent with the results in Section IV.A. This shows that the proposed constraint is effective. Also, it is

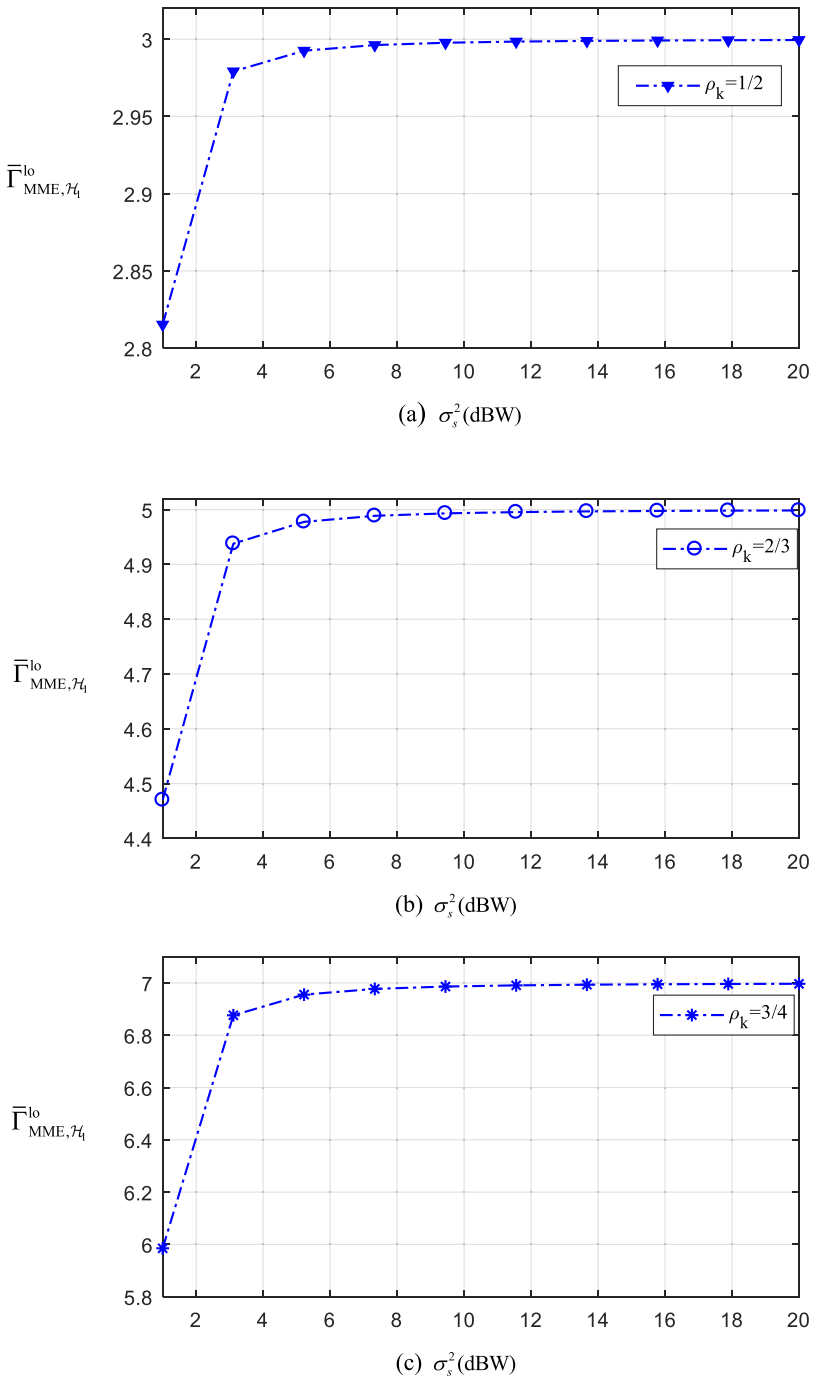

FIGURE 7. The transmitted power's effect on the bound of relative distance in SCFNR.

shown that the correlation coefficient ρ_k has fewer effects on the false-alarm probability and the missed-detection probability.

In short, the numerical results in Sections IV.B and IV.C show that to identify orbit elements for robust MME detector, the transmitter and receiver platforms remaining within some pre-specified relative distance for the entire mission lifetime in SCFNR, the condition in (34) must be satisfied. The results also show that controlling the orbit elements about the transmitter and receiver platforms in SCFNR can ensure MME robust and relative distance bounded.

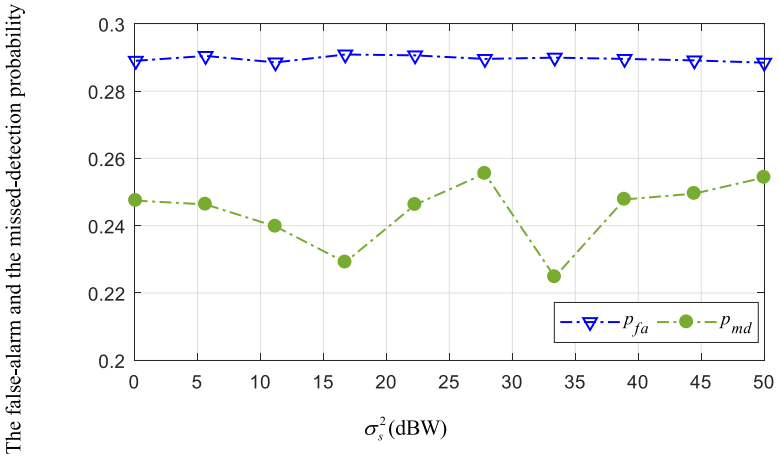

(a) $\rho_k = 1/2$

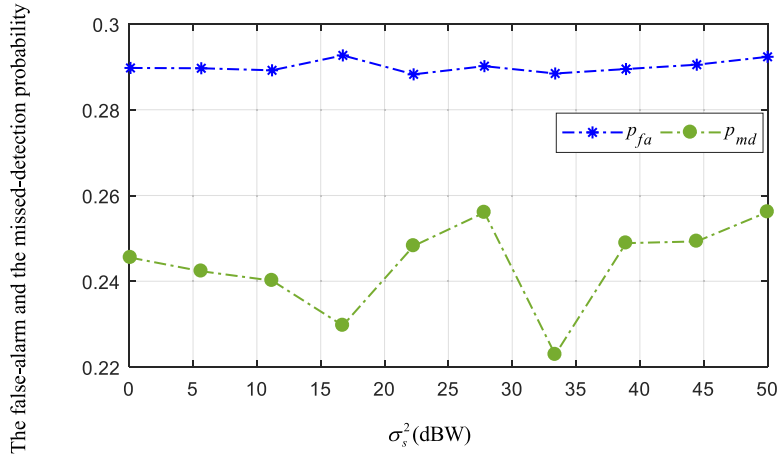

(b) $\rho_k = 2/3$

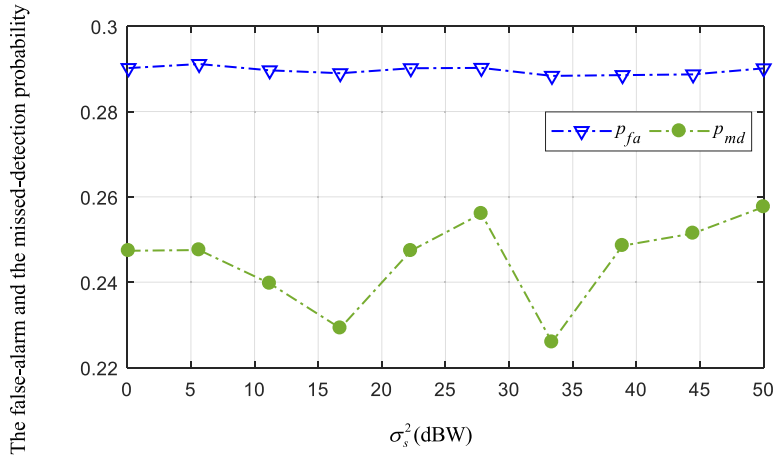

(c) $\rho_k = 3/4$

FIGURE 8. The relations between the transmitted power and the false-alarm probability, the missed-detection probability in SCFNR.

V. CONCLUSION

In this paper, we study the robust MME detection problem caused by the uncertainty of geometric configuration and focus on the constraint on bounded relative distance for robust MME detection in SCFNR. Firstly, according to the proposed novel concept of SCFNR, we have given the robust constraint condition about MME detector. Secondly, we have derived the closed-form of the lower bound on the test statistic under the presence of target return, the upper bound under the absence of target return. Next, the interval between the upper bound of transmitter-receiver distance and the lower bound in SCFNR for robust MME detecting, and the constraint on the bounded relative distance for robust MME detector have been given. Finally, the effectiveness of the proposed constraint have been validated through numerical calculations. The results have shown that controlling the orbit elements about the transmitter and receiver platforms in SCFNR can ensure the robustness of MME and relative distance bounded.

In the future, to further develop the theory and application of SCFNR, we will study problems on localization and tracking, etc.

APPENDIX

The proofs of theorems 1 and 2 are as follows:

Theorem 1: If the chief module C and the deputy module D of SCFNR have identical constant ballistic coefficients, if $\frac{\eta_{\max}-\eta_{\min}}{v_{\max}} \le \frac{\sin(|\Delta\Omega|/2)}{|\Delta t|}$, the difference between M and m satisfy (33).

$$\begin{aligned} 2v_{\min}|\Delta t| &\le M-m \\ &\le 2\eta_{\max}\sin\left(\frac{|\Delta\Omega|}{2}\right) \\ &\quad -2\eta_{\min}\sin\left(\frac{|\Delta\Omega|}{2}\right)+2v_{\max}|\Delta t| \end{aligned} \tag{A.1}$$

Proof: In [2], as the chief module C is met $v_{\min} \le v \le v_{\max}$ and $\eta_{\min} \le \eta \le \eta_{\max}$, then

$$\begin{aligned} &2\eta_{\min}\sin\left(\frac{|\Delta t|}{2}\right)-v_{\max}|\Delta t| \\ &\le m \le 2\eta_{\max}\sin\left(\frac{|\Delta t|}{2}\right)-v_{\min}|\Delta t| \\ &2\eta_{\min}\sin\left(\frac{|\Delta t|}{2}\right)+v_{\min}|\Delta t| \end{aligned} \tag{A.2}$$

$$\le M \le 2\eta_{\max}\sin\left(\frac{|\Delta t|}{2}\right)+v_{\max}|\Delta t| \tag{A.3}$$

In (A.2) and (A.3), the upper bound of m is less than or equal to the lower bound of M. This requires that

$$\frac{\eta_{\max}-\eta_{\min}}{v_{\max}} \le \frac{\sin(|\Delta\Omega|/2)}{|\Delta t|}.$$

Hence, if

$$\begin{aligned} \frac{\eta_{\max}-\eta_{\min}}{v_{\max}} &\le \frac{\sin(|\Delta\Omega|/2)}{|\Delta t|}, \\ 2\eta_{\max}\sin\left(\frac{|\Delta t|}{2}\right)-v_{\min}|\Delta t| &\\ \le 2\eta_{\min}\sin\left(\frac{|\Delta t|}{2}\right)+v_{\min}|\Delta t|, & \end{aligned}$$

and (A.2) and (A.3) hold in the meantime.

Also, the (A.2) can be rewritten as follows:

$$\begin{aligned} &2\eta_{\min}\sin\left(\frac{|\Delta t|}{2}\right)-v_{\max}|\Delta t| \\ &\quad \le m \le 2\eta_{\min}\sin\left(\frac{|\Delta t|}{2}\right)-v_{\min}|\Delta t| \end{aligned} \tag{A.4}$$

From (A.3) and (A.4), we get

$$\begin{aligned} &2v_{\min}|\Delta t| \\ &\le M-m \le 2\eta_{\max}\sin\left(\frac{|\Delta\Omega|}{2}\right) \\ &\quad -2\eta_{\min}\sin\left(\frac{|\Delta\Omega|}{2}\right)+2v_{\max}|\Delta t| \end{aligned} \tag{A.5}$$

Q.E.D.

Theorem 2: In SCFNR, if the initial position of transmitter $S_{iT}(0)$ and mobility model $\mathrm{M}(t)$ are given, let $d_t^{\max} = \min\{d_p^{\max}\}, d_r^{\max} = \min\{d_q^{\max}\}$ and $d_t^{\min} = \min\{d_p^{\min}\}, d_r^{\min} = \min\{d_q^{\min}\}$, the MME detector is robust under the condition given by (29) when $0 < M - m \le 2 \cdot \frac{-b+\sqrt{b^2-4ac}}{a}$, where $C = \max\{C_p, C_q\}, D = \min\{C_p, C_q\}, a = \frac{20K_B\sigma_s^2\rho_k}{D^6} - \frac{20K_B\sigma_s^2}{C^6}, b = \frac{4K_B\sigma_s^2\rho_k}{D^5} + \frac{4K_B\sigma_s^2}{C^5}, c = \frac{K_B\sigma_s^2\rho_k}{D^4} - \frac{K_B\sigma_s^2}{C^4} - \sigma_u^2$.

Proof: In SCFNR, to make sure that the MME detector is robust, the following must be satisfied (A.6), as shown at the bottom of the page. In fact, (A.7), as shown at the bottom of the page, also (A.8) and (A.9), as shown at the top of the next page.

$$\min\left\{\sigma_u^2+\frac{K_B\sigma_s^2}{\|d_p(0)\|^2\|d_q(0)\|^2}-\frac{\rho_k K_B\sigma_s^2}{\|d_p(0)\|\|d_q(0)\|\|d_p(k)\|\|d_q(k)\|}\right\}>0, \quad \forall p,q \tag{A.6}$$

$$\begin{aligned} &\min\left\{\sigma_u^2+\frac{K_B\sigma_s^2}{\|d_p(0)\|^2\|d_q(0)\|^2}-\frac{\rho_k K_B\sigma_s^2}{\|d_p(0)\|\|d_q(0)\|\|d_p(k)\|\|d_q(k)\|}\right\} \\ &=\sigma_u^2+K_B\sigma_s^2\min\left\{\frac{1}{\|d_p(0)\|^2\|d_q(0)\|^2}\right\}+K_B\sigma_s^2\rho_k\min\left\{-\frac{1}{\|d_p(0)\|\|d_q(0)\|\|d_p(k)\|\|d_q(k)\|}\right\} \end{aligned} \tag{A.7}$$

$$\min\left\{\frac{1}{\left\|d_p(0)\right\|^2\left\|d_q(0)\right\|^2}\right\}=\frac{1}{\left|d_p^{\max}d_q^{\max}\right|^2}=\frac{1}{\left(C_p+R\right)^2\left(C_q+R\right)^2}$$
$$\geq\frac{1}{\left(\max\left\{C_p,C_q\right\}+R\right)^2\left(\max\left\{C_p,C_q\right\}+R\right)^2}=\frac{1}{(C+R)^4}\tag{A.8}$$

$$\min\left\{-\frac{1}{\left\|d_p(0)\right\|\left\|d_q(0)\right\|\left\|d_p(k)\right\|\left\|d_q(k)\right\|}\right\}=-\frac{1}{\left|d_p^{\min}d_q^{\min}\right|^2}=-\frac{1}{\left(C_p-R\right)^2\left(C_q-R\right)^2}$$
$$\geq-\frac{1}{\left(\min\left\{C_p,C_q\right\}-R\right)^2\left(\min\left\{C_p,C_q\right\}-R\right)^2}=-\frac{1}{(D-R)^4}\tag{A.9}$$

$$\min\left\{\sigma_u^2+\frac{K_B\sigma_s^2}{\left\|d_p(0)\right\|^2\left\|d_q(0)\right\|^2}-\frac{\rho_k K_B\sigma_s^2}{\left\|d_p(0)\right\|\left\|d_q(0)\right\|\left\|d_p(k)\right\|\left\|d_q(k)\right\|}\right\}$$
$$\geq\sigma_u^2+K_B\sigma_s^2\frac{1}{(C+R)^4}-K_B\sigma_s^2\rho_k\frac{1}{(D-R)^4}\tag{A.10}$$

Generally, $R<D$, $R<C$. So, the (A.9) can be rewritten as (A.10), shown at the top of the page.

Expanding the right side of (A.10) in Taylor series, and omitting the high order terms, the following is given by

$$\sigma_u^2+\frac{K_B\sigma_s^2}{C^4}\left(1-\frac{4R}{C}+\frac{20R^2}{C^2}\right)-\frac{K_B\sigma_s^2\rho_k}{D^4}\times\left(1+\frac{4R}{D}+\frac{20R^2}{D^2}\right)\geq 0\tag{A.11}$$

Due to $R>0$, and solving the (A.6), we get

$$0<M-m\leq 2\cdot\frac{-b+\sqrt{b^2-4ac}}{a}\tag{A.12}$$

REFERENCES

[1] L. Mazal and P. Gurfil, "Cluster flight algorithms for disaggregated satellites," *J. Guid., Control, Dyn.*, vol. 36, no. 1, pp. 124–135, Jan. 2013.
[2] A. Kandhalu and R. Rajkumar, "QoS-based resource allocation for next-generation spacecraft networks," in *Proc. IEEE 33rd Real-Time Syst. Symp.*, Dec. 2012, pp. 163–172.
[3] S. Nag, C. K. Gatebe, and O. de Weck, "Observing system simulations for small satellite formations estimating bidirectional reflectance," *Int. J. Appl. Earth Observ. Geoinf.*, vol. 43, pp. 102–118, Dec. 2015.
[4] R. Palamá, M. Greco, and F. Gini, "Multistatic adaptive CFAR detection in non-Gaussian clutter," *EURASIP J. Adv. Signal Process.*, vol. 2016, no. 1, pp. 1–17, Dec. 2016.
[5] V. Amanipour and A. Olfat, "CFAR detection for multistatic radar," *Signal Process.*, vol. 91, no. 1, pp. 28–37, Jan. 2011.
[6] H. Y. Zhao, Z. J. Zhang, J. Liu, S. Zhou, J. Zheng, and W. Liu, "Target detection based on F-test in passive multistatic radar," *Digit. Signal Process.*, 79, pp. 1–8, Oct. 2018.
[7] Y. Zhao, Z. Yongjun, and C. Zhao, "A novel algebraic solution for moving target localization in multi-transmitter multi-receiver passive radar," *Signal Process.*, vol. 143, pp. 303–310, Feb. 2018.
[8] X. Zhang, H. Li, and B. Himed, "Multistatic detection for passive radar with direct-path interference," *IEEE Trans. Aerosp. Electron. Syst.*, vol. 53, no. 2, pp. 915–925, Apr. 2017.
[9] A. R. Persico, P. Kirkland, C. Clemente, J. J. Soraghan, and M. Vasile, "CubeSat-based passive bistatic radar for space situational awareness: A feasibility study," *IEEE Trans. Aerosp. Electron. Syst.*, vol. 55, no. 1, pp. 476–485, Feb. 2019.
[10] S. Saillant, "ExoMars spacecraft detection with European space surveillance bistatic radar," in *Proc. CIE Int. Conf. Radar*, Guangzhou, China, Oct. 2016, pp. 1–5.
[11] M. F. Xia, "Effects of geometry configurations on ambiguity function for cluster flight netted radar," *Chin. J. Space Sci.*, vol. 39, pp. 816–823, Oct. 2019.
[12] T. T. Yan, S. Hu, J. Cai, and M. Xia, "Optimization of transmitter-receiver pairing of spaceborne cluster flight netted radar for area coverage and target detection," *Math. Problems Eng.*, vol. 2021, Mar. 2021, Art. no. 8863000.
[13] D. R. Kartchner and S. K. Jayaweera, "A modified test statistic for maximum-minimum eigenvalue detection based on asymptotic distribution thresholds," in *Proc. Moratuwa Eng. Res. Conf. (MERCon)*, Moratuwa, Sri Lanka, May 2018, pp. 25–30.
[14] Y. Zeng and Y.-C. Liang, "Maximum-minimum eigenvalue detection for cognitive radio," in *Proc. IEEE 18th Int. Symp. Pers., Indoor Mobile Radio Commun.*, Athens, Greece, Sep. 2007, pp. 1–5.
[15] A. Kortun, T. Ratnarajah, M. Sellathurai, Y.-C. Liang, and Y. Zeng, "On the eigenvalue-based spectrum sensing and secondary user throughput," *IEEE Trans. Veh. Technol.*, vol. 63, no. 3, pp. 1480–1486, Mar. 2014.
[16] M. Shbat and V. Tuzlukov, "Primary signal detection algorithms for spectrum sensing at low SNR over fading channels in cognitive radio," *Digit. Signal Process.*, vol. 93, pp. 187–207, Oct. 2019.
[17] L. Wei, Z. Zheng, A. Hero, and V. Tarokh, "Scaling laws and phase transitions for target detection in MIMO radar," in *Proc. IEEE Inf. Theory Workshop (ITW)*, Cambridge, U.K., Sep. 2016, pp. 345–348.
[18] Y. Jiang, Y. Wang, Y. Li, and X. Chen, "Eigenvalue-based ground target detection in high-resolution range profiles," *IET Radar Sonar Navigat.*, vol. 14, pp. 1747–1756, Dec. 2020.
[19] W. Zhao, Z. Chen, and M. Jin, "Subband maximum eigenvalue detection for radar moving target in sea clutter," *IEEE Geosci. Remote Sens. Lett.*, vol. 18, no. 2, pp. 281–285, Feb. 2021.
[20] A. Bollig, C. Disch, M. Arts, and R. Mathar, "SNR walls in eigenvalue-based spectrum sensing," *EURASIP J. Wireless Commun. Netw.*, vol. 2017, no. 1, pp. 1–17, Dec. 2017.
[21] R. B. Chaurasiya and R. Shrestha, "Hardware-efficient and fast sensing-time maximum-minimum-eigenvalue-based spectrum sensor for cognitive radio network," *IEEE Trans. Circuits Syst. I, Reg. Papers*, vol. 66, no. 11, pp. 4448–4461, Nov. 2019.

[22] T. Yan, S. Hu, and J. Mo, "Path formation time in the noise-limited fractionated spacecraft network with FDMA," *Int. J. Aerosp. Eng.*, vol. 2018, pp. 1–12, Oct. 2018.
[23] J. Huang, Y. Su, L. Huang, W. Liu, and F. Wang, "An optimized snapshot division strategy for satellite network in GNSS," *IEEE Commun. Lett.*, vol. 20, no. 12, pp. 2406–2409, Dec. 2016.
[24] A. Bollig, C. Disch, M. Arts, and R. Mathar, "SNR walls in eigenvalue-based spectrum sensing," *EURASIP J. Wireless Commun. Netw.*, vol. 2017, no. 1, p. 109, Dec. 2017.
[25] N. J. Willis and H. D. Griffifiths, "Advances in bistatic radar (book review)," *IEEE Aerosp. Electron. Syst. Mag.*, vol. 23, no. 7, p. 46, 2008.
[26] A. Papoulis and S. U. Pillai, "Probability, random variables and stochastic processes," in *McGraw-Hill Higher Education*. New York, NY, USA: McGraw-Hill, 2002.

MINGFEI XIA received the B.Sc. degree in measurement control from the Equipment Command and Technology College, Beijing, China, in 2003, and the M.Sc. degree in software engineering from Sichuan University, Sichuan, China, in 2010. He is currently pursuing the Ph.D. degree with the School of Mathematical Science, Guizhou Normal University, Guiyang, China. His current research interests include radar system analysis and simulation and radar signal processing.

SHENGBO HU received the B.Sc. degree in communication engineering from Southeast University, Nanjing, China, in 1985, the M.Sc. degree in communication engineering from the National University of Defense Technology, Changsha, China, in 1992, and the Ph.D. degree in communication engineering from Chongqing University, Chongqing, China in 2006. He is currently a Professor and the Dean with the School of Big Data and Computer Science, Guizhou Normal University, China. He has been funded as a member of the Academic Committee of the Key Laboratory of Electronic and Information Technology for Complex Space Systems, CAS. His current research interests include radar system analysis and simulation, radar signal processing, and radar target detection.

TINGTING YAN received the B.Sc. and M.Sc. degrees from the School of Mechanical and Electrical Engineering, Guizhou Normal University, Guiyang, China, in 2014 and 2017 respectively, and the Ph.D. degree from the School of Mathematical Science, Guizhou Normal University, in 2021. She is currently a Teacher with the School of Big Data and Computer Science, Guizhou Normal University. Her current research interests include optimization theory, radar system analysis and simulation, and radar target detection.

YANFENG SHI, photograph and biography not available at the time of publication.

JIANAN CAI, photograph and biography not available at the time of publication.